CHEMICAL ENGINEERING TRANSACTIONS
VOL. 101, 2023
A publication of AIDIC
The Italian Association of Chemical Engineering
Online at www.cetjournal.it
Guest Editors: Paolo Ciambelli, Luca Di Palma

ISBN 979-12-81206-00-7; **ISSN** 2283-9216
DOI: 10.3303/CET23101009

Role of the Structure of TiO_2 Nanoparticles Synthesized by a Sol-Gel Reactor With Ultra-Rapid Micromixing on Photocatalytic Properties

Alex Lemarchand*, Lounis Bekkar, Oriana Haddad, Mamadou Traore, Mehrdad Nikravech, Andrei Kanaev

Laboratoire des Sciences des Procédés et des Matériaux, CNRS, Université Sorbonne Paris Nord, 93430 Villetaneuse, France
alex.lemarchand@lspm.cnrs.fr

TiO_2 nanoparticles were prepared via sol-gel method using a chemical reactor with ultra-rapid micromixing. The as-formed nanoparticles atomic structure was characterized using the pair distribution function method and compared to the structure of several titanium oxide based compounds (anatase, rutile, brookite, Ti-lepidocrocite-type). The best agreement was obtained with the Ti-lepidocrocite-type structure. Connection between photocatalytic properties and atomic structure of the nanoparticles was discussed.

1. Introduction

In the actual context of high-level pollution of both air and water, the development of efficient photocatalysts able to degrade pollutants is a major field of research (Ohtani, 2010a) (Parrino et al., 2019). Titanium dioxide (TiO_2) nanostructured materials are one of the most efficient photocatalysts and have been widely studied (Hashimoto et al., 2005). TiO_2 is a wide band gap semiconductor (E_g=3.0-3.2 eV) activated under UV light illumination. Most of the studies have been dedicated to the crystalline TiO_2 phases since amorphous phase was generally considered as inactive. In fact, only a few reports showed a negligible activity of the amorphous TiO_2 phase. This is attributed to the inherent structural disorder of the amorphous phase, facilitating recombination of photoinduced electron-hole pairs (Ohtani et al., 1997). However, a very thin disordered layer is always present at the catalytic surface that can critically affect the activity (Soria et al., 2017). Photocatalytic activity is strongly correlated to physical properties of TiO_2 such as crystal structure, surface area, particles size, etc. (Nakata and Fujishima, 2012). Among these properties, crystal structure of TiO_2 (anatase, rutile, brookite, amorphous) is supposed to be the most essential criterion to predict the photocatalytic properties, since anatase has far higher photocatalytic activity than rutile or amorphous phases. In a previous study of the group, Benmami *et al.* proposed an example of efficient non-crystalline TiO_2 nanocatalyst (Benmami et al., 2006). Thin nanocoatings were prepared by chemical deposition of small TiO_2 nanoparticles (~5.0 nm) on glass supports from a monodispersed colloidal suspension synthesized in a chemical sol-gel reactor with ultra-rapid micromixing. These nanocoatings showed a great ability to degrade trichloroethylene in the gas phase with an increased photocatalytic activity comparable with the best commercial crystalline powders. A high surface-to-volume ratio of nanoparticles, total active surface accessible and role of support in the charge separation process were the main explanation of these surprising high photocatalytic activity. Original structural features induced by the synthesis method could also be responsible of the increase of photocatalytic activity of these nanocoatings. These structural properties require further investigation with appropriate methods. In the present communication, we report on structural characterization of the primary TiO_2 nanoparticles used to prepare the photocatalytic nanocoatings developed by Benmami *et al.* (Benmami et al., 2006). The pair distribution function (PDF) method was used to reveal the local order of the very small primary TiO_2 nanoparticles synthesized in the sol-gel T-mixer with ultrarapid micromixing. This method is especially valuable since in nanoparticles lacking of long-range order conventional XRD methods are inefficient to

Paper Received: 20 January 2023; Revised: 29 March 2023; Accepted: 30 May 2023
Please cite this article as: Lemarchand A., Bekkar L., Haddad O., Traore M., Nikravech M., Kanaev A., 2023, Role of the Structure of TiO_2 Nanoparticles Synthesized by a Sol-gel Reactor with Ultra-rapid Micromixing on Photocatalytic Properties, Chemical Engineering Transactions, 101, 49-54 DOI:10.3303/CET23101009

provide reliable structural information about local arrangement (Billinge, 2019). The experimental PDF was compared and refined against structural models of several TiO_2 based compounds of anatase, brookite, rutile, Ti-lepidocrocite-type. The photocatalytic properties of the nanocoatings were rediscussed regarding the nature of the primary TiO_2 nanoparticle's structure.

2. Experimental

2.1 Chemicals

Titanium (IV) tetraisopropoxide (TTIP) with 98% purity and n-propanol with 99.5 % purity were purchased from Sigma-Aldrich. Distillated water (H_2O) was filtered twice using syringe filter 0.2 µm porosity PALLs Acrodiscs).

2.2 Material preparation

The titanium oxide nanoparticles were prepared *via* a sol-gel method in a chemical reactor with ultra-rapid micromixing (Azouani et al., 2009). The reactor used for the TiO_2 synthesis nanoparticles has been described in previous studies of the team (Rivallin et al., 2005). All manipulations concerning the solution preparation were carried out in a LABstar glovebox workstation MBraun under dry N_2 atmosphere ($O_2 \leq 0.5$ ppm, $H_2O \leq 0.5$ ppm) to avoid any contamination by air humidity and dust particles promoting heterogeneous precipitation of reactive colloids. Two stock solutions of 50 mL each containing A) TTIP in n-propanol and B) water in n-propanol were prepared. The Ti^{4+} concentration (C_{Ti}) was fixed to 0.3 M and the water concentration (C_W) was chosen to obtain hydrolysis ratio ($h = C_w/C_{Ti}$) of 2.0. Each solution A) and B) were transferred via glass syringes of 50 mL volume each to the reactor containers maintained under dry nitrogen flow to prevent any contamination of the reactive media from environment. The solutions were then injected in the exocentric T-mixer though two input tubes of 1 mm diameter and the mixed solution exited the mixer through the main tube output of 2 mm diameter. The injection was triggered by applying a dry nitrogen gas pressure to the reactor containers by synchronous valves opening. The reactions began at the contact of the injection stock solutions in a T-mixer. The fluids were injected with a rate of 10 m/s (at the applied pressure of 4 bars) corresponding to a strong turbulent flow in the mixing zone with Reynolds number Re = 6000 ($Re = 4Qp/\pi\eta d$, where Q, p and η are flow rate, density and dynamic viscosity of the fluid respectively), forcing the solutions to mix at the molecular level on a timescale t_{mix}<10 ms, which is shorter than the characteristic time of chemical reactions resulting in the particles nucleation t_{nuc}. This reactor regime corresponds to so-called small Damköhler numbers $Da = t_{mix}/t_{nuc} \leq 1$, which assure point-like conditions in the reaction medium with perfectly homogeneous composition. These optimal conditions also permit the narrowest polydispersity of the produced nanoparticles. The reactor was maintained at the temperature of 20 °C with a thermocryostat Haake DC10K15. The time of the stock solutions preparation and transfer to the thermostatic reactor after the glove box operations was about 25 min. This procedure leads to the formation of stable colloidal suspension of very small TiO_2 primary nanoparticles. The typical nanoparticles size obtained using the procedure described above has been estimated 2R≤5nm *via* Dynamic Light Scattering (DLS) measurements in previous studies of the team (Azouani et al., 2009). The nanoparticles powders required for the structural characterization were then obtained from the colloidal suspension by solvent evaporation at ambient temperature. This step does not modify the atomic structure of the primary TiO_2 nanoparticles. White powders were finally collected and softly grounded for the following structural characterization.

2.3 Total scattering measurements, data processing and atomic pair distribution function analysis

Atomic pair distribution function. The reduced atomic PDF is defined as:

$$G(r) = 4\pi\left[\rho(r)-\rho_0\right] \quad (1)$$

where $\rho(r)$ and ρ_0 are the local and average atomic number densities and *r* the radial distance.

The PDF signal, G(r), thus corresponds to the probability of finding a pair of atoms at a distance *r* in the structure and it may be described as a real space one-dimensional function showing positive peaks at *r* values corresponding to characteristics interatomic distance in the sample. PDF method provides quantitative structural information about local structural order including all the deviations from the average structure (Egami and Billinge, 2012). This method is powerful regarding the structural analysis of disordered materials.

The PDF of a sample can be obtained experimentally from total scattering (TS) X-ray measurements. After correction and normalization of raw data, the structure factor S(Q) is extracted from TS measurements. The experimental atomic PDF G(r) is finally obtained as a function of radial distance *r* through Fourier transform of the structure factor:

$$G_{exp}(r) = \frac{2}{\pi}\int_0^{\infty} Q[S(Q)-1]\sin(Qr)\,dQ \quad (2)$$

where Q corresponds to the magnitude of the scattering vector. Q is defined as:

$$Q = \frac{4\pi\sin(\theta)}{\lambda} \quad (3)$$

with 2θ, the angle between the incident and diffused X-rays and λ the wavelength of the X-rays beam (Egami and Billinge, 2012).

Total scattering measurements and data processing. Total scattering (TS) measurements were performed at the high-energy beamline station P21.1, DESY, PETRA III, Germany. The X-ray wavelength was 0.122244 Å and the sample-to-detector distance was ~389mm. The exact distance was calibrated using a LaB_6 powder standard. A few tens of milligrams of TiO_2 nanoparticles powders were placed into a thin wall 1 mm diameter borosilicate capillary and positioned in a capillary sample holder. The capillary holder was positioned inside a chamber under vacuum at ambient temperature for transmission TS X-ray measurements. TS patterns were acquired with a Q scattering vector range of 0.2-30 Å. The TS patterns were captured by a Perkin Elmer plate detector, with integration of the circularly symmetric scattering pattern about the transmitted beam direction. The TS pattern of empty capillary was also acquired for background subtraction. Calibration and integration were performed using Dioptas software (Prescher and Prakapenka, 2015). The structure factor S(Q) of the sample was derived from experimental TS patterns after suitable data reduction. S(Q) is finally Fourier-transformed into the experimental PDF $G_{exp}(r)$. Data reduction and correction were performed using PDFgetx3 software (Juhás et al., 2013). TS data were used for powder X-ray diffraction (PXRD) pattern and for the PDF analysis.*PDF data analysis*. The refinements of the experimental PDF of the TiO_2 nanoparticles were performed using PDFfit 2 software implemented in its PDFgui interface (Farrow et al., 2007). The structural models of the rutile, the brookite, the anatase and Ti-lepidocrocite-type were obtained from literature and refined against the experimental PDF data. In each case, cell parameters, atomic positions, atomic displacements factors, particle size attenuation factor and scale factor were refined.

3. Results and discussion

The synchrotron PXRD pattern for the as-synthesized TiO_2 nanoparticles is shown in Figure 1.

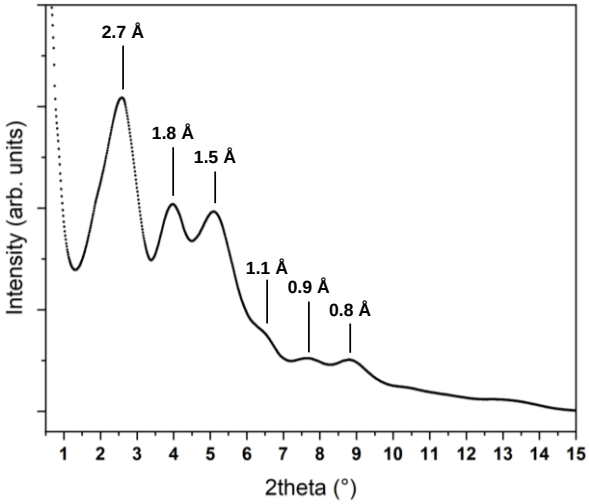

Figure 1: Synchrotron PXRD pattern for as-synthesized TiO_2 nanoparticles (λ = 0.122244 Å) d-spacing shown.

The PXRD pattern only shows very broad humps at corresponding d-spacing values of 2.7 Å, 1.8 Å, 1.5 Å with several much weaker very broad contributions. This features are typical of an amorphous sample with very small coherence domains and in line with the characteristics of the very small as-synthesized TiO_2 nanoparticles (2R< 5 nm). However, it is impossible to further analyze the PXRD pattern to obtain structural information using conventional XRD methods since it is very diffuse in nature.

To overcome this limitation, PDF analysis method was used to investigate the local atomic structure of the TiO_2 nanoparticles. The experimental PDF of the as-synthesized TiO_2 nanoparticles is shown in Figure 2. The first peak in the PDF of the as-synthesized TiO_2 nanoparticles visible at 1.93 Å is quite narrow. It corresponds to the Ti-O distance in Ti-O_6 octahedra, which are the main constituting units in most of the TiO_2 polymorphs such as anatase, brookite, rutile structure and also amorphous TiO_2. This first observation shows that Ti-O_6 octahedra are already formed inside the as-synthesized nanoparticles. Several less intense peaks are

observed up to 7.0 Å, which corresponds to middle range order and to the distances between first octahedral units in the structure. For higher r values, the signal tends to 0 corresponding to a total loss of coherence. The estimated coherence length was thus estimated to 10 Å. As this distance is lower than the nanoparticle size, it appears that the nanoparticle structure is heavily disordered. The experimental PDF presented here is comparable to those reported by Gateshki et al. (Gateshki et al., 2007) and Grey et al. (Grey et al., 2021).

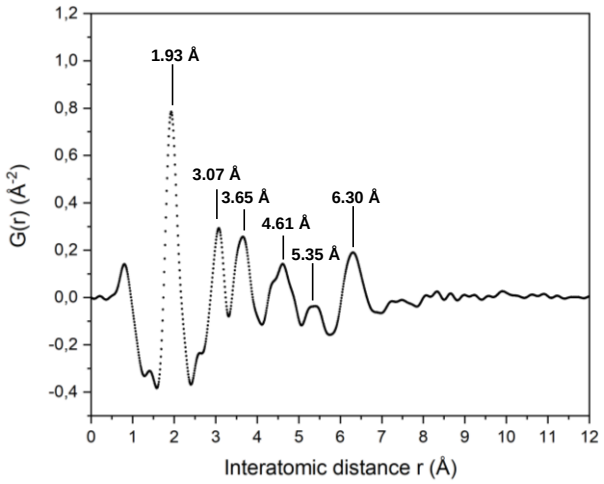

Figure 2: Atomic PDF of as-synthesized TiO_2 nanoparticles.

The experimental PDF was then compared to the three main TiO_2 polymorphs, i.e. rutile, anatase and brookite which can be described as a 3D network of TiO_6 octahedra edge- and corner-shared with precise corner to edge connection ratio, and to the protonated Ti-lepidocrocite, $H_xTi_{2-x/4}O_4$, which has a layered structure built from edge- and corner-shared octahedra with an interlayer distance of ~ 9 Å (Sasaki et al., 1995). Those structures are then all built of interconnected TiO_6 octahedra but with different number of neighboring units. The calculated PDF from each models were simulated on the basis of unit-cell constants and atomic positions found in the literature. The very limited coherence length was taken into account by applying an attenuation factor corresponding to a very small particle size of around 10 Å. The results are shown in Figure 3.

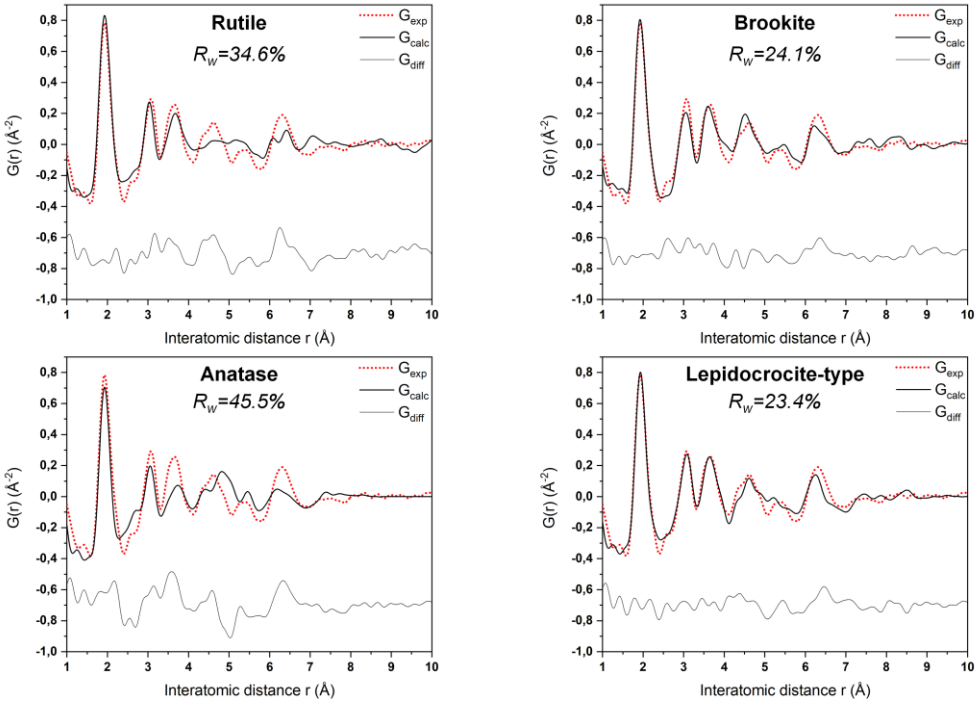

Figure 3: Experimental PDF of as-synthesized TiO_2 nanoparticles (red dot) compared with model PDFs (thick black line) based on the rutile, anatase, brookite and lepidocrocite-type structures. Residuals are shown by gray line. R_w values are given for each refinement.

All the calculated PDF simulate quite well the two first peaks of the experimental PDF, which correspond respectively to the first Ti-O and Ti-Ti distances, confirming that the nanoparticles are composed of TiO_6 octahedral units. However for higher r values, the agreement between the simulated and experimental PDF is getting worse, in particular for rutile (R_w=34.6%) and anatase (R_w=45.5%) models. Knowing that applying a 450°C heat treatment to those particles leads to their conversion into anatase (Mendez et al., 2021), this result is surprising and imply that important restructuring process seems to occur during the crystallization of the nanoparticles. For the calculated PDF from brookite models, the agreement is better (R_w=24.1%). However, the best agreement was obtained for the model based on Ti-lepidocrocite-type structure (R_w=23.4%). This observation indicates that the 3D network of connected TiO_6 octahedra is closer to the Ti-lepidocrocite-type one. However, the agreement between the experimental and calculated PDF is not perfect meaning that the model is not able to explain all the structural characteristics observed in the real nanoparticle atomic structure. The results of the structural characterization of the as-synthesized nanoparticles are close to those structure observed Gateshki et al. (Gateshki et al., 2007) and Grey et al. (Grey et al., 2021). They concluded that their material was composed of nanosize fragments of TiO_6 octahedra connected according to the coupling scheme observed in Ti-lepidocrocite type structure. We assume that this description is also well-suited for the as-synthesized TiO_2 nanoparticles obtained in the sol-gel reactor with rapid micro-mixing. Finally, the structure of the as-synthesized TiO_2 nanoparticles is in accordance with that is usually described for amorphous TiO_2 nanoparticle in literature.

The photocatalytic activity of nanocoatings elaborated from these amorphous TiO_2 nanoparticles has been studied earlier by Benmami et al. (Benmami et al., 2006) in the case of the trichloroethylene degradation in the gas phase using a continuous-flow fix-bed reactor under UV illumination. Nanocoatings were obtained putting into contact support and colloidal suspension of reactive primary TiO_2 nanoparticles produced by sol-gel reactor with rapid micromixing. They have reported that the photocatalytic activity of these nanocoatings was higher than of the industrial product Degussa P-25 TiO_2, which is composed of a mixture of anatase (70%), rutile (30%) TiO_2 and a small but not negligible amorphous component (Ohtani et al., 2010b). Moreover, they have shown that the film thickness was a crucial parameter that can influence the material efficiency, as it relates to the internal traps population. By reducing it to the thinnest submonolayer of amorphous TiO_2 nanoparticles, the best intrinsic performances were obtained. As amorphous TiO_2 was supposed to show only a negligible activity, these results are very interesting. In a recent review, Sun et al. highlighted some unique physical and chemical properties of the amorphous TiO_2 which could be of great interest in the field of photocatalysis (Sun et al., 2019). In particular, the presence of structural defects and oxygen vacancies inherent to the structural disorder state of the nanoparticle could promote photochemical applications improving the conductivity of charge holder. It is thus probable that the high photocatalytic properties observed for the nanocoatings based on amorphous TiO_2 nanoparticles synthesized in the sol-gel reactor with micromixing rely on thin film characteristics, in particular on its very low thickness, provided by the reactive chemical colloidal deposition developed by Benmami et al. and on the unique chemical and physical properties of the amorphous TiO_2 nanoparticles.

4. Conclusion

The atomic structure of very small amorphous TiO_2 nanoparticles synthesized in a sol-gel reactor with ultra-rapid micromixing was analysed by the mean of PDF method. The experimental PDF was in line with an amorphous network composed of relatively well-defined TiO_6 octahedra with a coherence length limited to 8-9 Å. The experimental PDF was compared to simulated PDF calculated from structural model of rutile, anatase, brookite and Ti-lepidocrocite type. The best agreement was obtained with the Ti-lepidocrocite-type structural model meaning that the structural middle range order in the TiO_2, i.e. the first TiO_6 octahedra coupling, was close to the Ti-lepidocrocite-type structure. The structure of the amorphous TiO_2 nanoparticles could then be described as a disordered network of TiO_6 octahedra connected in the coupling scheme of the Ti-lepidocrocite structure. The inherent structural disorder in the amorphous TiO_2 nanoparticles could promote in some way their photocatalytic activity by increasing the conductivity of charge carriers during the photochemical processes. Further investigations are required to investigate the photochemical processes occurring during photocatalysis.

Acknowledgements

We acknowledge DESY (Hamburg, Germany), a member of the Helmholtz Association HGF, for the provision of experimental facilities. Parts of this research were carried out at PETRA III and we would like to thank Dr. Ida Gjerlevsen Nielsen for assistance in using P21.1 beamline. Beamtime was allocated for proposal I-20211531 EC.

References

Azouani, R., Tieng, S., Michau, A., Hassouni, K., Chhor, K., Bocquet, J.F., Vignes, J.L., Kanaev, A., 2009. Elaboration of doped and composite nano-TiO_2 Chemical Engineering Transactions 17, 981–986.

Benmami, M., Chhor, K., Kanaev, A.V., 2006. High photocatalytic activity of monolayer nanocoatings prepared from non-crystalline titanium oxide sol nanoparticles. Chemical Physics Letters 422, 552–557.

Billinge, S.J.L., 2019. The rise of the X-ray atomic pair distribution function method: a series of fortunate events. Philosophical Transactions of the Royal Society A: Mathematical, Physical and Engineering Sciences 377, 20180413.

Egami, T., Billinge, S.J.L., 2012. Underneath the Bragg Peaks: Structural Analysis of Complex Materials. Newnes.

Farrow, C.L., Juhas, P., Liu, J.W., Bryndin, D., Božin, E.S., Bloch, J., Proffen, T., Billinge, S.J.L., 2007. PDFfit2 and PDFgui: computer programs for studying nanostructure in crystals. Journal of Physics: Condensed Matter 19, 335219.

Gateshki, M., Yin, S., Ren, Y., Petkov, V., 2007. Titania Polymorphs by Soft Chemistry: Is There a Common Structural Pattern? Chemistry of Materials 19, 2512–2518.

Grey, I.E., Bordet, P., Wilson, N.C., 2021. Structure of the amorphous titania precursor phase of N-doped photocatalysts. RSC Advances 11, 8619–8627.

Hashimoto, K., Irie, H., Fujishima, A., 2005. TiO_2 Photocatalysis: A Historical Overview and Future Prospects. Japanese Journal of Applied Physics 44, 8269.

Juhás, P., Davis, T., Farrow, C.L., Billinge, S.J.L., 2013. PDFgetX3: a rapid and highly automatable program for processing powder diffraction data into total scattering pair distribution functions. Journal of Applied Crystallography 46, 560–566.

Mendez, M.S., Lemarchand, A., Traore, M., Amar, M.B., Perruchot, C., Nikravech, M., Kanaev, A., 2021. Preparation and Photocatalytic Activity of Coatings Based on Size-selective V-TiO_2 Nanoparticles. Chemical Engineering Transactions 84, 19–24.

Nakata, K., Fujishima, A., 2012. TiO_2 photocatalysis: Design and applications. Journal of Photochemistry and Photobiology C: Photochemistry Reviews 13, 169–189.

Ohtani, B., 2010a. Photocatalysis A to Z—What we know and what we do not know in a scientific sense. Journal of Photochemistry and Photobiology C: Photochemistry Reviews 11, 157–178.

Ohtani, B., Ogawa, Y., Nishimoto, S., 1997. Photocatalytic Activity of Amorphous−Anatase Mixture of Titanium(IV) Oxide Particles Suspended in Aqueous Solutions. Journal of Physical Chemistry B 101, 3746–3752.

Ohtani, B., Prieto-Mahaney, O.O., Li, D., Abe, R., 2010b. What is Degussa (Evonik) P25? Crystalline composition analysis, reconstruction from isolated pure particles and photocatalytic activity test. Journal of Photochemistry and Photobiology A: Chemistry 216, 2-3, 179–182.

Parrino, F., Loddo, V., Augugliaro, V., Camera-Roda, G., Palmisano, G., Palmisano, L., Yurdakal, S., 2019. Heterogeneous photocatalysis: guidelines on experimental setup, catalyst characterization, interpretation, and assessment of reactivity. Catalysis Reviews 61, 163–213.

Prescher, C., Prakapenka, V.B., 2015. DIOPTAS: a program for reduction of two-dimensional X-ray diffraction data and data exploration. High Pressure Research 35, 223–230.

Rivallin, M., Benmami, M., Kanaev, A., Gaunand, A., 2005. Sol–Gel Reactor With Rapid Micromixing: Modelling and Measurements of Titanium Oxide Nano-particle Growth. Chemical Engineering Research and Design 83, 67–74.

Sasaki, T., Watanabe, M., Michiue, Y., Komatsu, Y., Izumi, F., Takenouchi, S., 1995. Preparation and Acid-Base Properties of a Protonated Titanate with the Lepidocrocite-like Layer Structure. Chemistry of Materials 7, 1001–1007.

Soria, J., Sanz, J., Torralvo, M.J., Sobrados, I., Garlisi, C., Palmisano, G., Çetinkaya, S., Yurdakal, S., Augugliaro, V., 2017. The effect of the surface disordered layer on the photoreactivity of titania nanoparticles. Applied Catalysis B: Environmental 210, 306–319.

Sun, S., Song, P., Cui, J., Liang, S., 2019. Amorphous TiO_2 nanostructures: synthesis, fundamental properties and photocatalytic applications. Catalysis Science and Technology 9, 4198–4215.